Nonlinear benchmarking between CLT and M3D-C1

W. Zhang[1], S. C. Jardin[2] , Z. W. Ma[1,a)], A. Kleiner[2], and H. W. Zhang[1]

[1]Institute for Fusion Theory and Simulation, Department of Physics, Zhejiang University, Hangzhou 310027, China

[2]Princeton Plasma Physics Laboratory, P.O. Box 451, Princeton, New Jersey 08543, USA

Abstract: A systematical benchmarking between the CLT code and the M3D-C1 code is presented, including the nonlinear tearing mode and resistive-kink mode. CLT is an explicit finite difference code, while M3D-C1 is an implicit finite element code. Although the implementations of CLT and M3D-C1 are totally different, we find that the simulation results of the resistive-kink mode and the m/n=2/1 tearing mode from M3D-C1 and CLT are quantitatively the same, including the linear and nonlinear growth rates, the mode structures, the nonlinear saturation levels, the Poincare plots, and the scaling laws. This confirms that the simulation results of the MHD instabilities are only determined by the equilibrium and boundary conditions, and are independent of the code implementations and the initial perturbations. This, in turn, implies that the nonlinear results of the two codes are correct and accurate.

[a)] Corresponding Author: zwma@zju.edu.cn

I. Introduction

Tearing modes are common phenomena in tokamaks. The tearing modes are the primary cause of the degradation of tokamak performance[1] and even disruptions.[2] Sawteeth, which not only flatten the plasma temperature but also may trigger neo-classical tearing modes in nearby resonant surfaces,[3, 4] are believed to be related to the nonlinear evolution of the resistive-kink mode.[5, 6] It is worthwhile to investigate these instabilities to increase our understanding with the goal of achieving high-performance operation in future fusion reactors.[7, 8]

The resistive tearing mode was first studied by Furth et al., who found that the linear growth rate scales as $\gamma \sim S^{-3/5}$, where S is the Lundquist number. [9] The first analytical theory of the resistive-kink mode was that by by Coppi et al. [6], who found that the linear growth rate scales as $\gamma \sim S^{-1/3}$. Not only linear studies but also nonlinear theoretical studies have been reported in the past decades.[10-12] It should be noted that significant simplification of the physical model and the geometry is applied in these theoretical analytical studies. To confirm that these assumptions are reasonable and to gain more insight into those instabilities, simulation studies have been widely conducted. [13, 14] Since the implementation of different codes are different,[15-19] and the nonlinear evolution from different simulation codes sometimes are significantly different, it is difficult to say which simulations are correct.

One way to verify the simulation results is to quantitatively benchmark between different codes. This method can be effective, but it is still a challenge since the nonlinear simulation results can be sensitive to many details of the formulation, the equilibrium, the boundary conditions and the initial conditions. The M3D-C1 code is an implicit, three-dimensional high-order finite-element code for the solution of the time-dependent linear or nonlinear two-fluid magnetohydrodynamic (MHD) equations in cylindrical or toroidal geometry.[17] The CLT code is an explicit three-dimensional finite-difference nonlinear MHD code for toroidal geometry.[19] Although they are both used to investigate MHD instabilities in tokamaks, the

implementations in the two codes are totally different. Quantitative benchmarking the two codes on several problems could demonstrate that the simulation results of both codes are accurate. In the present paper, the benchmarking between CLT and M3D-C1, including the linear and nonlinear evolution of the tearing modes and the resistive-kink mode, is presented.

II. Model descriptions, normalizations, and code implementations.

Before the benchmarking between CLT and M3D-C1, we have to make sure that the physical model used in the two codes are the same. A brief introduction of the two codes is presented in this subsection. It should be noted that both of the codes could include two-fluid MHD effects. While, in the present paper, we only use the single-fluid model, a benchmarking with the two-fluid MHD model will be the subject of future work.

The single-fluid MHD model used in CLT[19] and M3D-C1.[20] is as follows:

$$\frac{\partial \rho}{\partial t} = -\nabla \cdot (\rho \mathbf{v}) + \nabla \cdot [D \nabla (\rho - \rho_0)] \tag{1.1}$$

$$\frac{\partial p}{\partial t} = -\mathbf{v} \cdot \nabla p - \Gamma p \nabla \cdot \mathbf{v} + \nabla \cdot [\kappa_\perp \nabla_\perp (p - p_0)] + \nabla \cdot [\kappa_\parallel \hat{\mathbf{b}} \hat{\mathbf{b}} \cdot \nabla p] \tag{1.2}$$

$$\frac{\partial \mathbf{v}}{\partial t} = -\mathbf{v} \cdot \nabla \mathbf{v} + (\mathbf{J} \times \mathbf{B} - \nabla p) / \rho + \nabla \cdot [\nu \nabla (\mathbf{v})] \tag{1.3}$$

$$\frac{\partial \mathbf{B}}{\partial t} = -\nabla \times \mathbf{E} \tag{1.4}$$

$$\mathbf{E} = -\mathbf{v} \times \mathbf{B} + \eta (\mathbf{J} - \mathbf{J}_0) \tag{1.5}$$

$$\mathbf{J} = \frac{1}{\mu_0} \nabla \times \mathbf{B} . \tag{1.6}$$

Here ρ , p, $\mathbf{v}$, $\mathbf{B}$, $\mathbf{E}$, and $\mathbf{J}$ are the mass density, the plasma pressure, the velocity, magnetic field, the electric field, and the current density, respectively. p_0 , ρ_0 , and $\mathbf{J_0}$ are the equilibrium plasma pressure, density, and current density, respectively.

$\Gamma(=5/3)$ is the ratio of specific heat of the plasma. Note that M3D-C1 actually time-advances the magnetic vector potential, **A**, and not **B,** but by taking the curl of the **A** equation, we obtain Eq. (1.4).

All variables are normalized as follows: $\mathbf{x}/L_0 \to \mathbf{x}$, $\rho/(n_0 M_i) \to \rho$, $p/(B_{00}^2/\mu_0) \to p$, $t/t_A \to t$, $\mathbf{v}/v_A \to \mathbf{v}$, $\mathbf{B}/B_{00} \to \mathbf{B}$, $\mathbf{E}/(v_A B_{00}) \to \mathbf{E}$, and $\mathbf{J}/(B_{00}/\mu_0 a) \to \mathbf{J}$ where $L_0 = 1$ m is the normal length, $B_{00} = 1$ T is the normal strength of the magnetic field, $n_0 = 1\times10^{20}\,\mathrm{m}^{-3}$ is the normal particle density, M_i is the mass of the ion, $v_A = B_{00}/\sqrt{\mu_0 n_0 M_i}$ is the Alfvén speed, and $t_A = L_0/v_A$ is the Alfvén time. The resistivity η and the diffusion coefficient D, the perpendicular and parallel thermal conductivity $\kappa_\perp$ and $\kappa_\parallel$, the viscosity ν are normalized as follows: $\eta/(\mu_0 L_0^{\,2}/t_A) \to \eta$, $D/(L_0^{\,2}/t_A) \to D$, $\kappa_\perp/(L_0^{\,2}/t_A) \to \kappa_\perp$, $\kappa_\parallel/(L_0^{\,2}/t_A) \to \kappa_\parallel$, and $\nu/(L_0^{\,2}/t_A) \to \nu$, respectively.

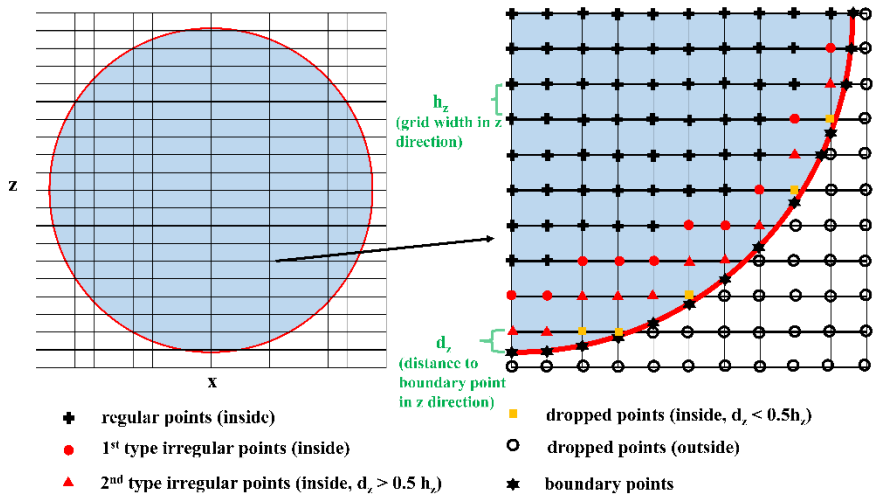

Figure 1 The schematic diagram of the cut-cell method. The grids are divided into 6 types, i. e. regular point : 4th order central finite difference (5 points, the boundary points are not required); 1st type irregular points: 4th order bias finite difference (5

points, the values at the boundary points are required); 2nd type irregular points: 4th order central finite difference (5 points, the values at the boundary points and the 1st type irregular points are required); dropped points (inside, $d_Z < 0.5h_Z$): not calculated in the specified dropped direction (because it is too close to the boundary point), but will be updated by linear interpolation for the requirement in another direction; dropped points (outside): not calculated; boundary points: fixed boundary condition is used at present, it will be updated to free boundary condition in the future.

Although CLT and M3D-C1 use the same physical model and cylindrical coordinate (R,φ,Z) to solve the toroidal tokamak geometry problems, the implementations in the codes are different. Firstly, the two codes use different methods for spatial discretization. The CLT code uses the fourth-order finite difference method in the R, φ, and Z directions, while the M3D-C1 code uses high-order triangular elements with continuous first derivatives (C^1 continuity) in the R and Z directions, and Hermite cubic finite elements in the φ direction.[17] In CLT, the grids are usually not located at the plasma boundary, which causes a significant problem for the code implementation. In the early version of CLT, we applied an interpolation method to solve the boundary problem.[21] However, this method reduces the parallel efficiency of the computation. Therefore, in the new version of the CLT code, we employ the cut-cell method [22] that is more efficient for parallelization. The schematic diagram of the cut-cell method can be seen from Figure 1. Along with the cut-cell method, we have also applied the OpenACC heterogeneous parallel programming model into the code, which typically makes the code 100 times faster.[19] The time advance methods in the two codes are also different. In CLT, the fourth-order accuracy Runge-Kutta explicit scheme is used for time advancing, while the θ-implicit method is used in M3D-C1. [17]

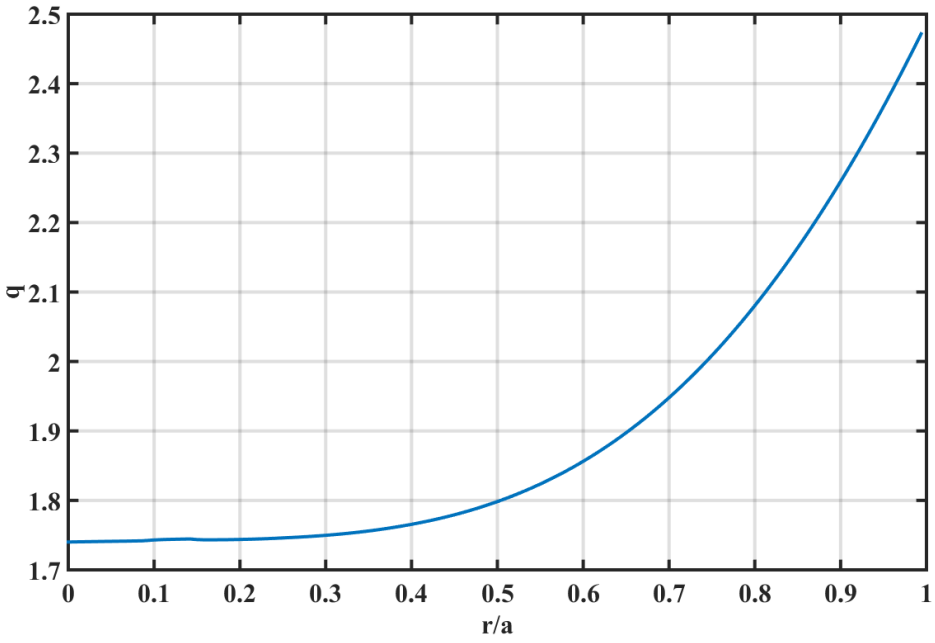

Figure 2 The initial safety factor profile used in the *m/n*=2/1 tearing mode benchmarking.

III. Benchmarking results.

In this subsection, we describe the linear and nonlinear benchmarking between CLT and M3D-C1 for two major tokamak instabilities: the resistive tearing mode and the resistive-kink mode.

A. The *m/n*=2/1 tearing mode

The initial safety factor profile for the *m/n*=2/1 tearing mode benchmarking is shown in Figure 2. The formula used for the *q*-profile is given as follows:

$$q = q_0 \times (1 + (\psi_n / q_l)^p)^{1/p} \tag{1.7}$$

Where ψ_n is the normalized poloidal flux, $q_0 = 1.75$, $q_e = 2.5$, $p = 2.0$, $q_l = ((q_e / q_0)^p - 1)^{-1/p}$, and $r = \sqrt{\psi_n}$. For simplification, the plasma beta and the aspect ratio are set to be $\beta \sim 0$ and $R/a = 10/1$ ($a = 1m$). The initial equilibrium is calculated by the QSOLVER code.[23] The dominant MHD instability in the system is the *m/n*=2/1 tearing mode.

The non-uniform mesh used in M3D-C1 is shown in Figure 3. During the simulation, we pack the mesh around the *q*=2 resonant surface to accurately simulate

the current sheet of the *m/n*=2/1 tearing mode. A total of 4800 elements in the poloidal plane and 16 toroidal planes are used in the nonlinear simulations. The 2D-complex version of M3D-C1 is used for the linear simulation, and the 3D nonlinear version is used for the nonlinear simulation. In CLT, the uniform grid $256\times16\times256$ (R,φ,Z) is used both for the linear and nonlinear simulations.

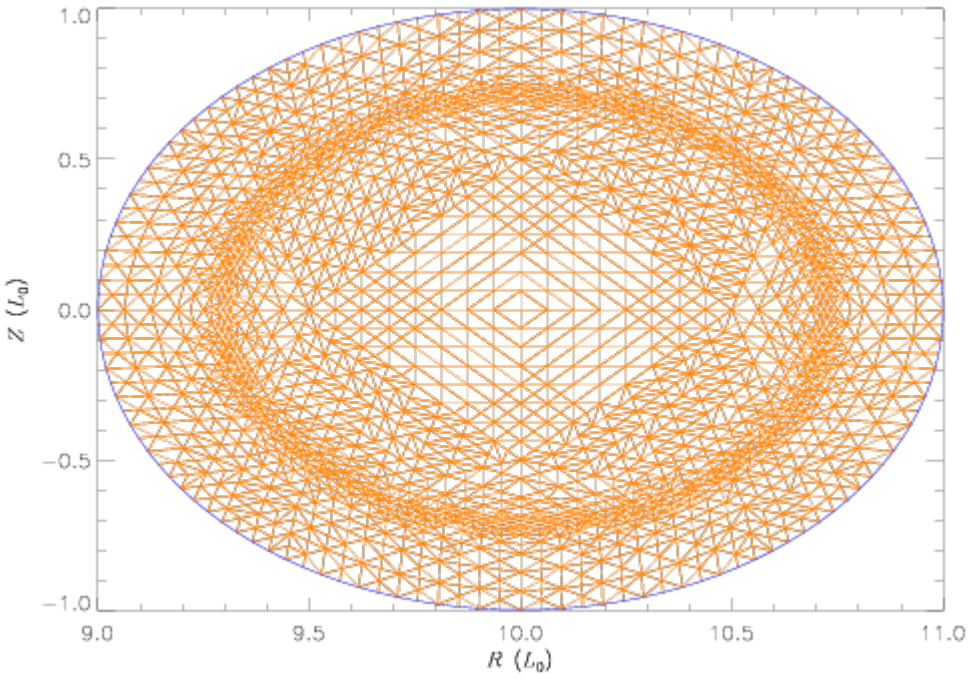

Figure 3 The non-uniform mesh used in the simulation of M3D-C1. We have packed the mesh around the *q*=2 resonant surface during the simulation.

We start with linear benchmarking the two codes. The diffusion parameters used in the linear benchmarking are $D=1.0\times10^{-8}$, $\nu=1.0\times10^{-8}$, $\kappa_{\perp}=1.0\times10^{-8}$, $\kappa_{\parallel}=0$. For simplification, we chose a constant resistivity and scanned from $\eta=1.0\times10^{-5}$ to $\eta=1.0\times10^{-7}$. The linear growth rates of the *m/n*=2/1 tearing mode with different resistivities are shown in Table 1. The difference between the linear growth rates from the two codes is about 10% for each case.

	$\eta = 1 \times 10^{-5}$	$\eta = 3 \times 10^{-6}$	$\eta = 1 \times 10^{-6}$	$\eta = 3 \times 10^{-7}$	$\eta = 1 \times 10^{-7}$
M3D-C1	**0.00178**	**0. 00116**	**0. 000675**	**0. 00033**	**0.000178**
CLT	**0.00165**	**0. 001044**	**0. 0006038**	**0. 000293**	**0.000135**

Table 1 The linear growth rates of the m/n=2/1 tearing mode with different resistivities. The time-steps are $dt \sim 8.5\times10^{-3} t_A$ in CLT and $dt = 1.0 t_A$ in M3D-C1, respectively. The difference between the linear growth rates from the two codes is about 10% for each case.

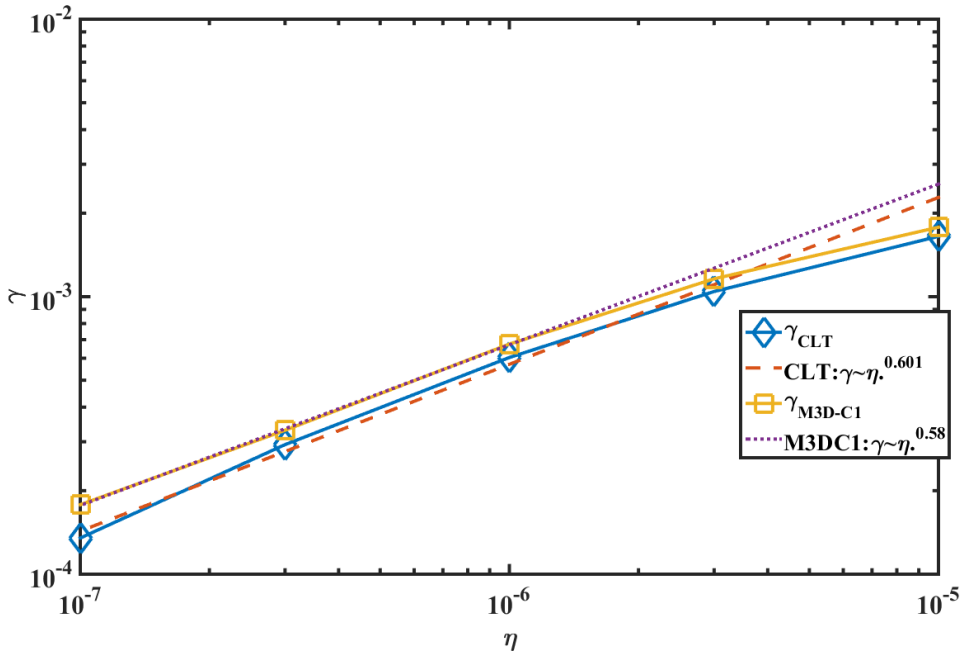

Figure 4 The scaling law of the linear growth rate on the resistivity for the tearing mode.

As shown in Figure 4, the scaling law for the linear growth rate with the resistivity is $\gamma \sim \eta^{0.601}$ in CLT and $\gamma \sim \eta^{0.58}$ in M3D-C1, which are both close to the asymptotic theoretical prediction,[9, 24] i.e., $\gamma \sim \eta^{3/5}$. For comparison of the eigenfunctions from the two codes, we use the linear toroidal electric field to represent the mode structure. As shown in Figure 5a and 5b, the mode structures from

the two codes are very similar, and both are the typical mode structures of the *m/n*=2/1 tearing mode.

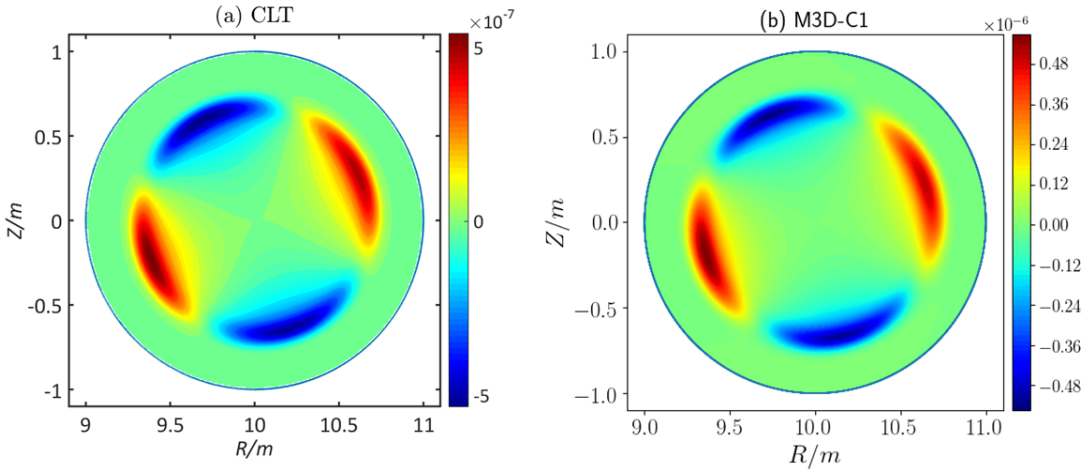

Figure 5 The toroidal electric field at the linear stage of the simulations (a) CLT and (b) M3D-C1, which represents the mode structure of the *m/n*=2/1 tearing mode.

The linear benchmarking of the *m/n*=2/1 tearing mode indicates that both codes work well for linear simulations of tearing modes. To ease computational requirements, we chose a constant resistivity $\eta = 1.0\times10^{-5}$ during the nonlinear simulations.

Because the equilibrium under consideration is large aspect ratio and zero β, the conditions for reduced MHD to be valid are well satisfied. We therefore used the 2-variable reduced MHD option in M3D-C1 where only the toroidal component of the magnetic vector potential ψ and the velocity stream function U are advanced in time. The vector potential and velocity at thus represented as:

$$\mathbf{A} = \psi\nabla\phi$$

$$\mathbf{V}=R^2\nabla U\times\nabla\phi$$

The nonlinear evolution of the kinetic energy for the *m/n*=2/1 tearing mode from the two codes is shown in Figure 6. The dominant mode in the system is the *n*=1 mode, and its amplitude is much larger than other harmonics. In the nonlinear stage,

the tearing mode finally saturates. The saturation level of the n=1 mode for the tearing mode in CLT is about 1.5×10^{-6}, while it is 1.4×10^{-6} in M3D-C1. The saturation levels for other harmonics from the two codes are also very close to each other.

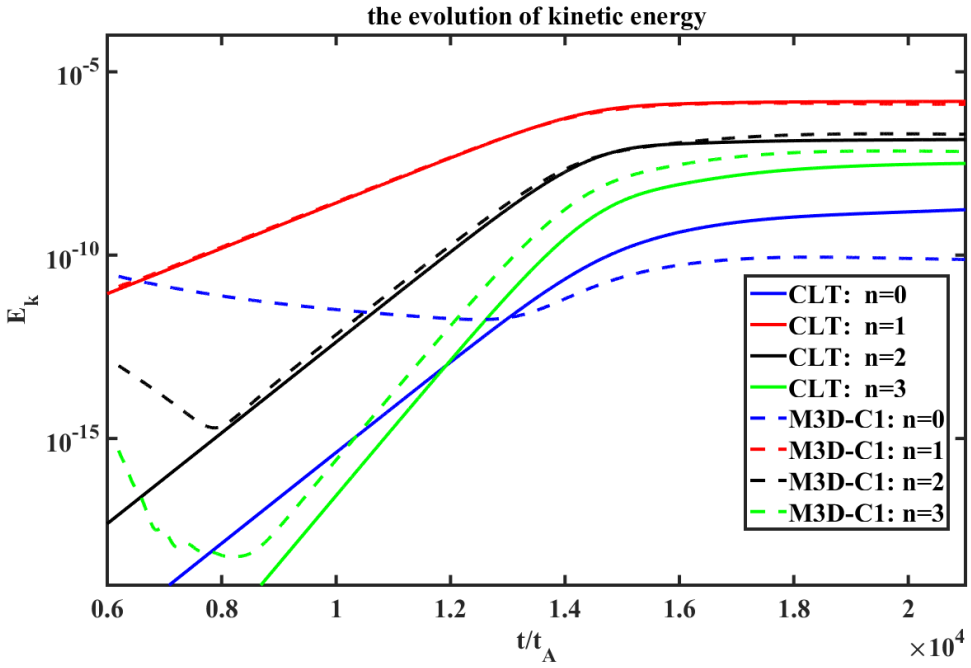

Figure 6 The nonlinear evolutions of the kinetic energy for the m/n=2/1 tearing mode from the two codes. The results from M3D-C1 are artificially shifted by $4200\,t_A$ for the purpose of the comparison.

The nonlinear evolutions of the growth rate for the m/n=2/1 tearing mode from the two codes are shown in Figure 7. The linear growth rates are γ=0.00143 in CLT and γ=0.00141 in M3D-C1, respectively. The growth rate of the n=1 mode initially stays almost unchanged during the long linear phase, but slowly reduces in the nonlinear phase, and finally becomes zero when the mode saturates.

In CLT, the initial perturbation only contains the n=1 component, and the n=1 mode is the dominant mode. During the linear stage, the other harmonics are solely driven beat modes of the n=1 mode. The growth rates of the n=2 and n=0 modes are twice that of the n=1 mode, and the growth rate of the n=3 mode is three times that of the n=1 mode. In M3D-C1, the initial perturbation is random and contains all

components. As a result, modes with different n are present from time zero. They initially decay, but eventually the beat components of the n=2 and n=3 modes become dominant when the n=1 mode grows to sufficient amplitude. The n=0 mode still independently develops, but its amplitude is much smaller than other modes (Figure 6), and is not important.

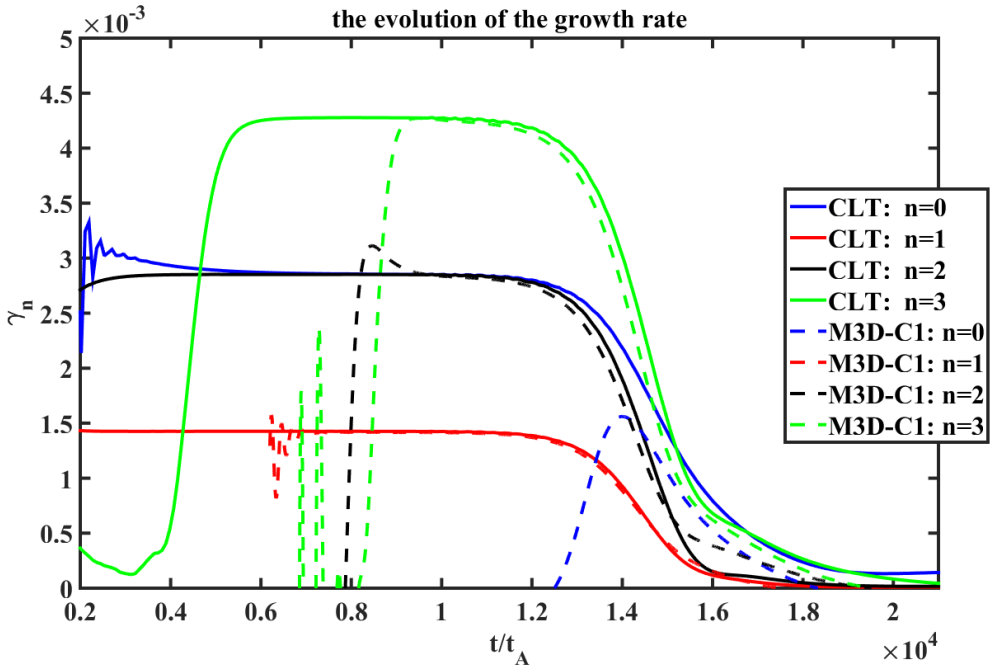

Figure 7 The nonlinear evolutions of the growth rate for the m/n=2/1 tearing mode from the two codes. The results from M3D-C1 are artificially shifted by $4200\,t_A$ for the purpose of the comparison.

As shown in Figure 8, the Poincare plots of the magnetic field at the saturation stage from the two codes are almost the same. The mode structures at the saturation stage are shown in Figure 9 (a) CLT and (b) M3D-C1, and are very similar.

Although the implementations in CLT and M3D-C1 are different and the tearing mode starts from different initial perturbations, the linear and nonlinear behavior and the saturation levels of the tearing mode from the two codes agree well each other. It indicates that the development of the tearing mode is independent of the code implementation and only determined by the initial equilibrium and the plasma parameters. This confirms that CLT and M3D-C1 are both excellent codes for tearing

mode studies. It also indicates that 2-variable reduced MHD provides an adequate description of this phenomena for these parameters.

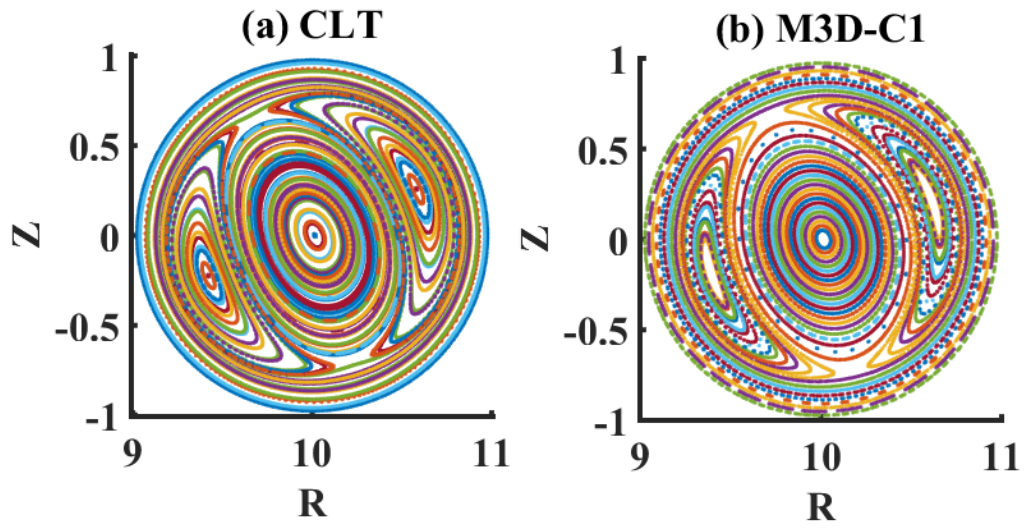

Figure 8 The Poincare plots of the magnetic field at the saturation stage from the two codes (a) CLT and (b) M3D-C1.

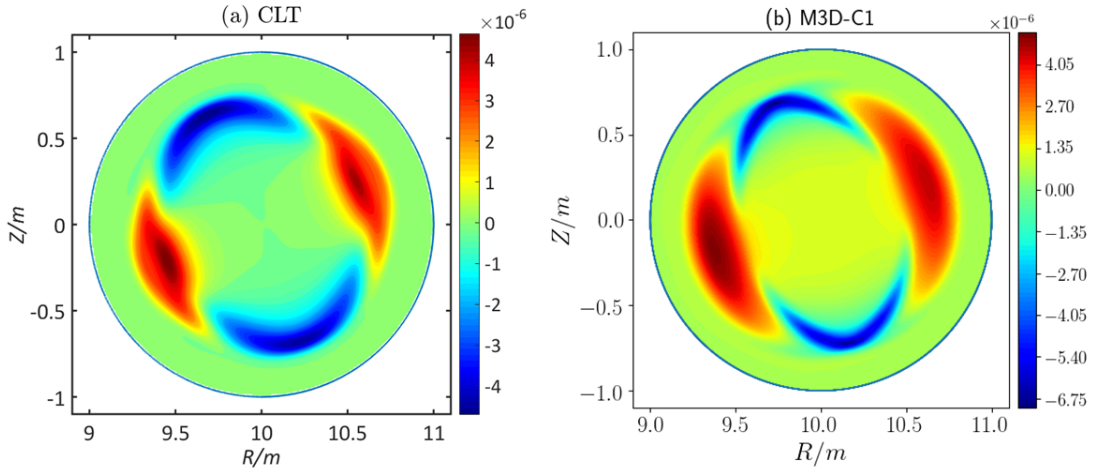

Figure 9 The mode structures at the saturation stage from the two codes (a) CLT and (b) M3D-C1.

B. The *m/n*=1/1 resistive-kink mode

The initial safety factor profile for the *m/n*=1/1 resistive-kink mode benchmarking is shown in Figure 10. The formula used in the QSOLVER code is

given as follows:

$$q = q_0 + \psi_n[q_e - q_0 + (q'_e - q_e + q_0)(1-\psi_s)(\psi_n - 1)/(\psi_n - \psi_s)] \quad (1.8)$$

Where $\psi_s = (q'_e - q_e + q_0)/(q'_e + q'_0 - 2q_e + 2q_0)$, $q_0 = 0.7$, $q_e = 3.6$, $q'_0 = 2.0$, and $q'_e = 5.0$. For simplification, the plasma beta and the aspect ratio are set to be $\beta \sim 0$ and $R/a = 10/1$ ($a = 1m$). The initial equilibrium is calculated by the QSOLVER code.[23] The *m/n*=1/1 resistive-kink mode is the dominant mode in the system.

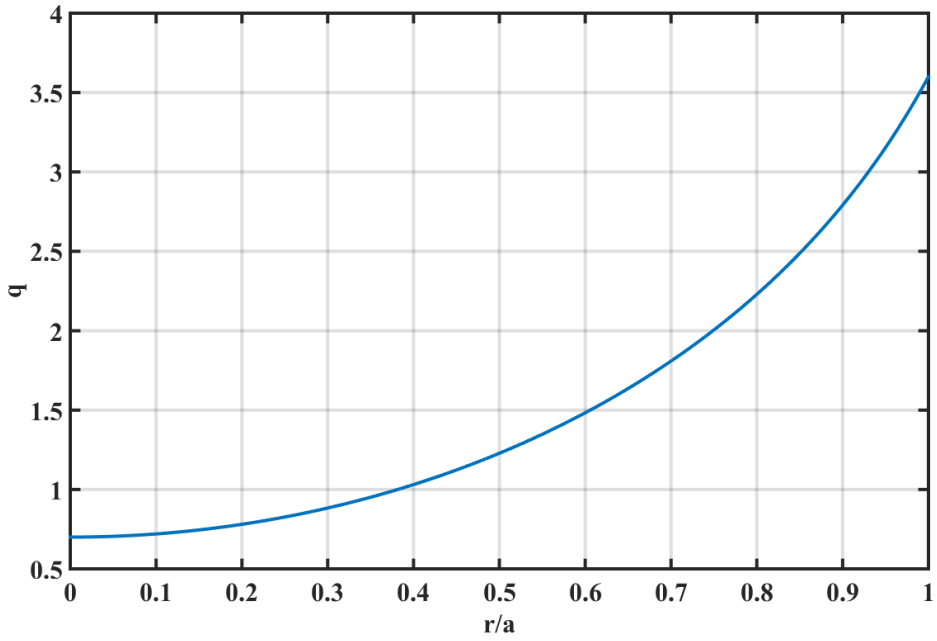

Figure 10 The initial safety factor profile used in the *m/n*=1/1 resistive-kink mode benchmarking.

The non-uniform mesh used in M3D-C1 is shown in Figure 11. We packed the mesh around the *q*=1 resonant surface to accurately simulate the current sheet of the *m/n*=1/1 resistive-kink mode. A total of 3816 elements in the poloidal plane and 12 toroidal planes were used in the nonlinear simulations. The 2D-complex version of M3D-C1 is used for the linear simulation, and the 3D nonlinear version is used for the nonlinear simulation. We again used the 2-variable reduced MHD model in M3D-C1 for the nonlinear calculation. In CLT, the uniform grid $256\times12\times256$ (R,φ,Z) are used both for the linear and nonlinear simulations.

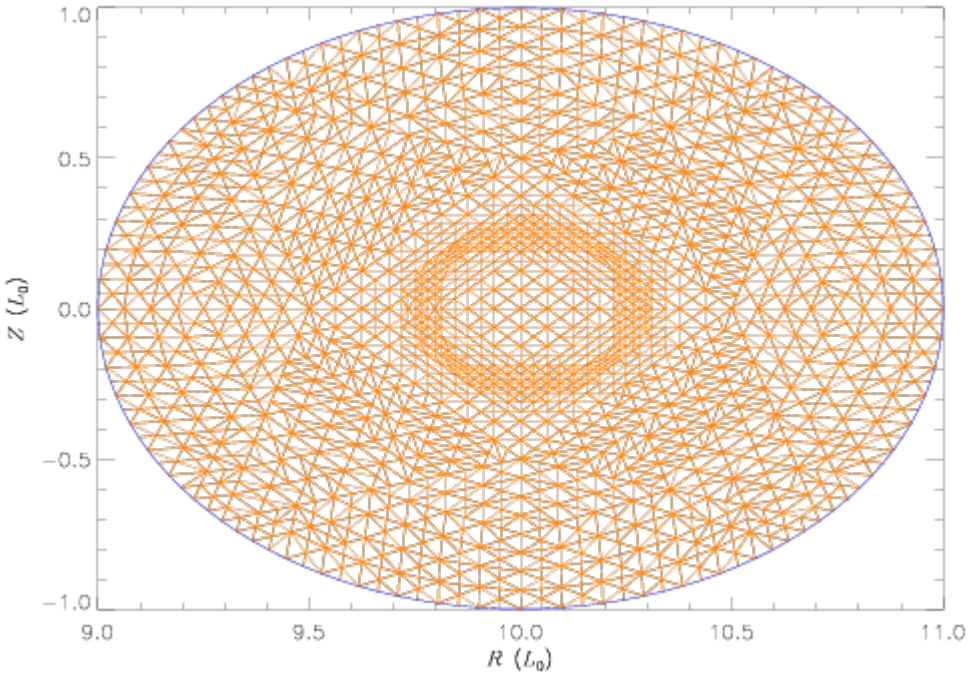

Figure 11 The non-uniform mesh used in the simulation of M3D-C1. We have dense the mesh around the q=1 resonant surface during the simulation.

Before the nonlinear benchmarking, a systematical linear scan with the two codes is carried out. The diffusion parameters used in the linear simulations are $D=1.0\times10^{-8}$, $\nu=1.0\times10^{-8}$, $\kappa_{\perp}=1.0\times10^{-8}$, $\kappa_{\parallel}=0$. For simplification, we chose a constant resistivity and scanned from $\eta=1.0\times10^{-5}$ to $\eta=3.0\times10^{-8}$. The linear growth rates of the m/n=1/1 resistive-kink mode with different resistivities are shown in Table 2. The difference between the linear growth rates from the two codes is about 5% for each case.

	$\eta=1\times10^{-5}$	$\eta=3\times10^{-6}$	$\eta=1\times10^{-6}$	$\eta=3\times10^{-7}$	$\eta=1\times10^{-7}$	$\eta=3\times10^{-8}$
M3D-C1	**0. 0115**	**0. 0087**	**0. 0064**	**0. 0044**	**0.0032**	**0. 0025**
CLT	**0. 01105**	**0. 008368**	**0. 006168**	**0. 004276**	**0.003**	**0. 002071**

Table 2 The linear growth rates of the m/n=1/1 resistive-kink mode with different

resistivities. The time-steps are $dt \sim 8.5\times10^{-3} t_A$ in CLT and $dt = 1.0 t_A$ in M3D-C1, respectively. The difference between the linear growth rates from the two codes is about 5% for each case.

As shown in Figure 12, the scaling laws for the linear growth rate with the resistivity are $\gamma \sim \eta^{0.31}$ in CLT and $\gamma \sim \eta^{0.30}$ in M3D-C1, respectively, which are both close to the asymptotic theoretical prediction,[6] i.e., $\gamma \sim \eta^{1/3}$. A qualitative comparison of the linear mode structures is shown in Figure 13. The mode structures in the two codes are both very similar to the typical mode structure of the *m*/*n*=1/1 resistive-kink mode.

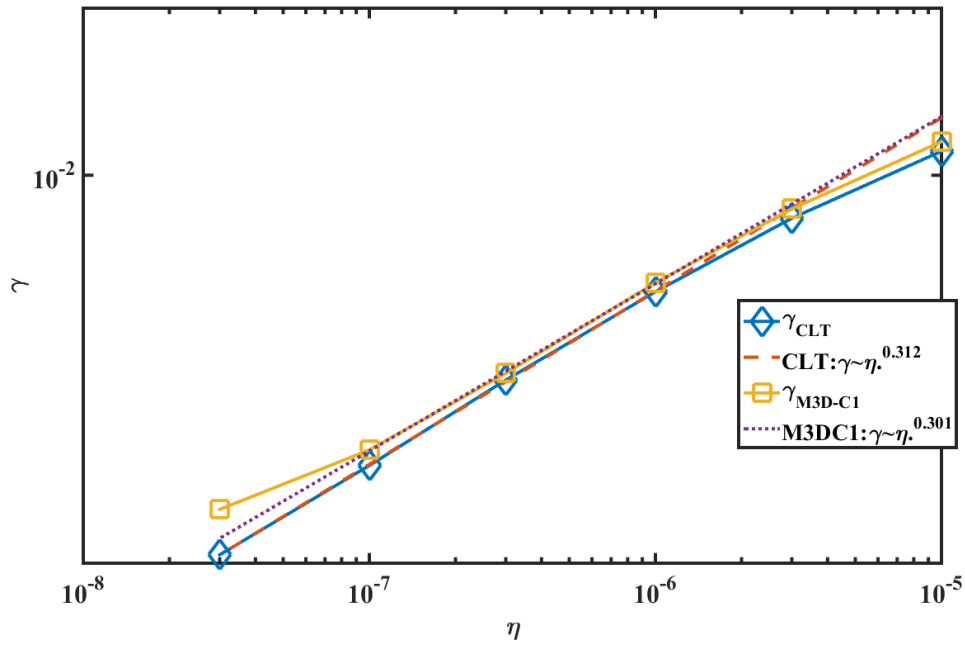

Figure 12 The scaling law of the linear growth rate on the resistivity for the resistive-kink mode.

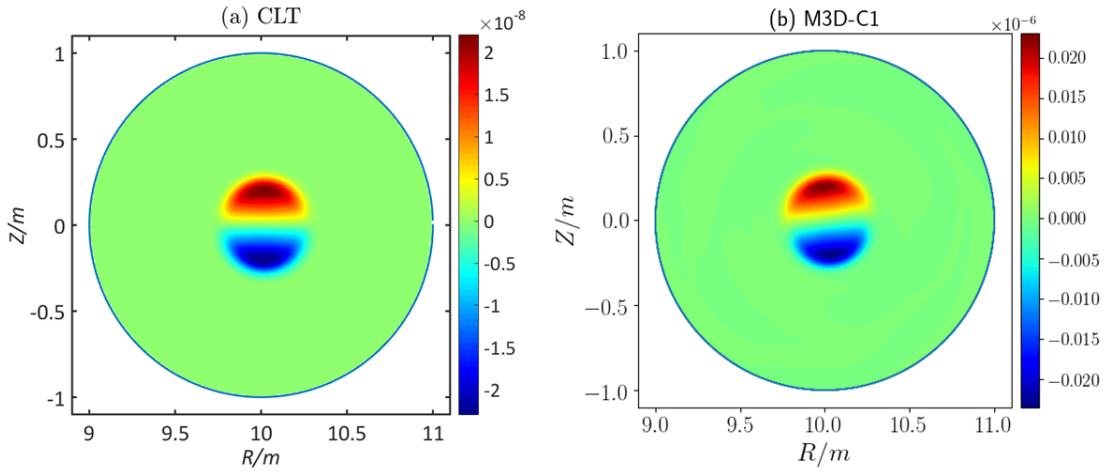

Figure 13 The toroidal electric field at the linear stage of the simulations (a) CLT and (b) M3D-C1, which represents the mode structure of the *m*/*n*=1/1 resistive-kink mode.

To again ease computing requirements we chose a constant resistivity $\eta = 1.0\times10^{-5}$ in the nonlinear simulations. The dominant mode is the *n*=1 mode, and its amplitude is much larger than other harmonics. As shown in Figure 14, the nonlinear evolution of the kinetic energy for the *m*/*n*=1/1 resistive-kink mode from the two codes is almost the same. During the nonlinear stage, the kinetic energy increases, saturates, and then decreases. The maximum value of the kinetic energy of the *n*=1 mode for the resistive-kink mode is 4.4×10^{-5} in CLT, while it is 4.2×10^{-5} in M3D-C1. The behavior of the other harmonics in the two codes is also very similar.

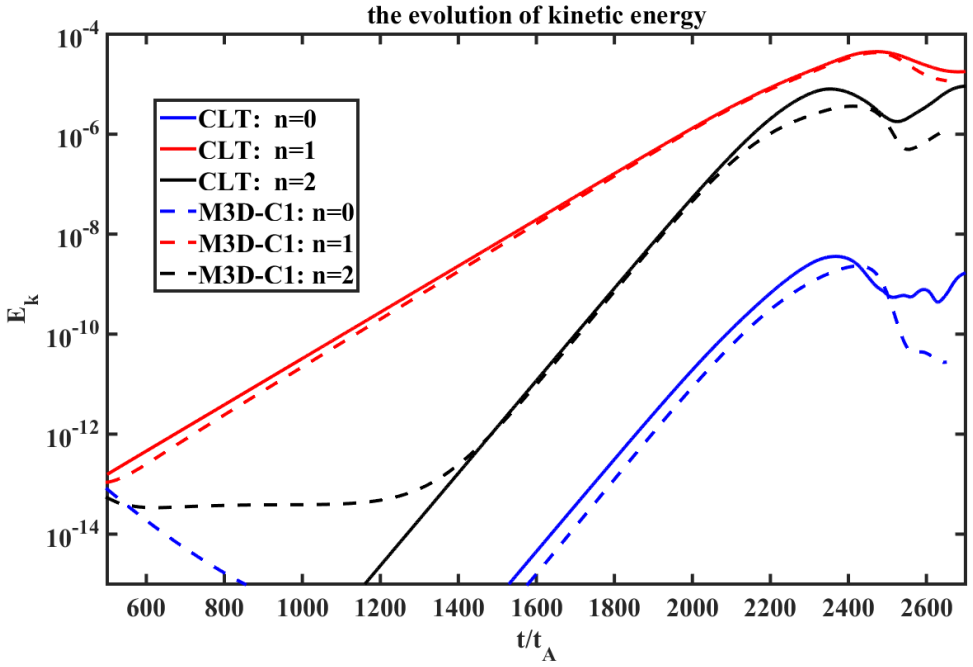

Figure 14 The nonlinear evolutions of the kinetic energy for the m/n=1/1 resistive-kink mode from the two codes. The results from M3D-C1 are artificially shifted by $270\,t_A$ for the purpose of the comparison.

As shown in Figure 15, the linear growth rates of the n=1 mode are γ=0.0107 in CLT and γ=0.011 in M3D-C1. In both codes, the growth rates of the n=1 mode initially stays almost unchanged during the long linear phase, then slowly reduces in the early nonlinear phase, and then suddenly reduces to a negative value. It should be pointed out that the evolution of the growth rates are still qualitatively the same even after the crash.

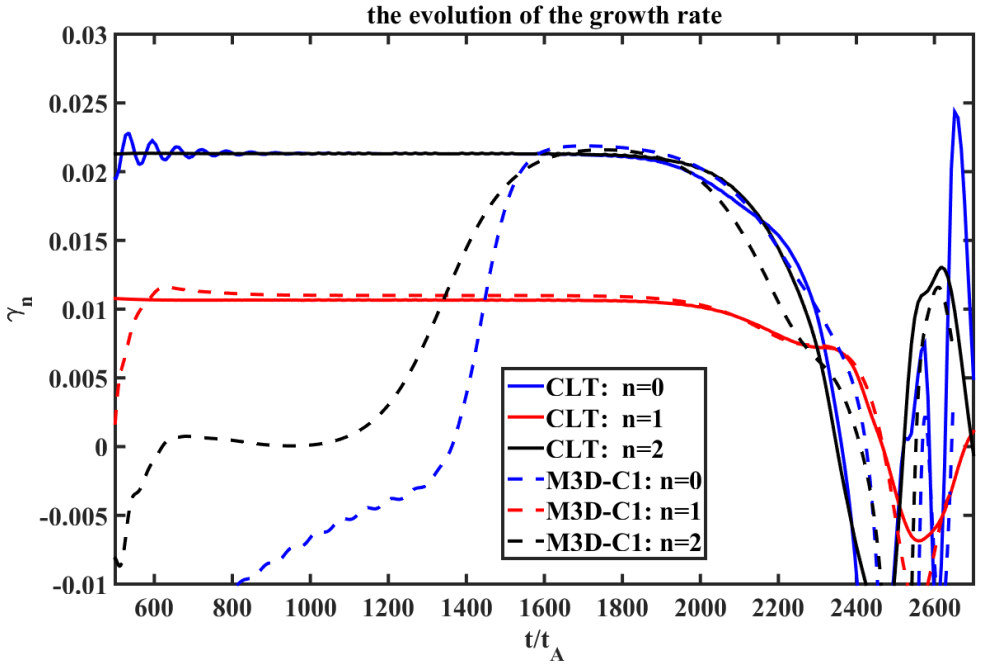

Figure 15 The nonlinear evolutions of the growth rate for the *m*/*n*=1/1 resistive-kink mode from the two codes. The results from M3D-C1 are artificially shifted by $270\,t_A$ for the purpose of the comparison.

The Poincare plots of the magnetic field during the nonlinear stage from the two codes are shown in Figure 16 (a) CLT and (b) M3D-C1. They are almost the same. The corresponding mode structures are shown in Figure 17 (a) CLT and (b) M3D-C1.

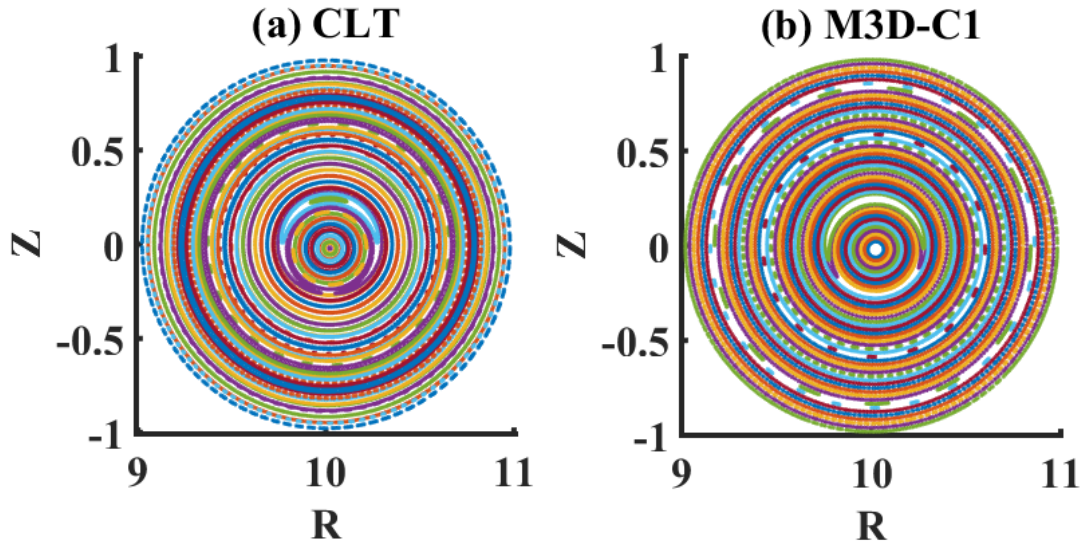

Figure 16 The Poincare plots of the magnetic field at the nonlinear stage from the two

codes (a) CLT and (b) M3D-C1.

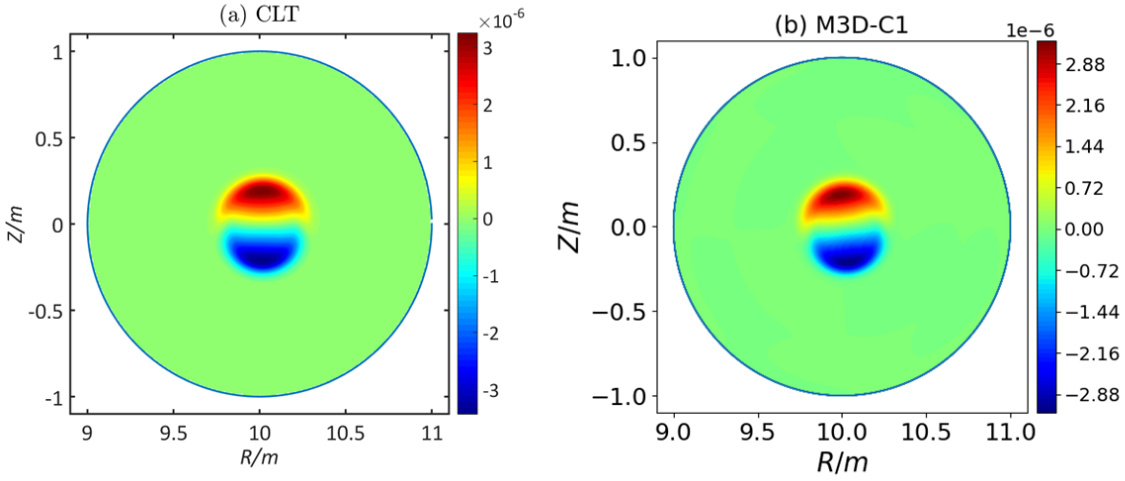

Figure 17 The toroidal electric field at the nonlinear stage from the two codes (a) CLT and (b) M3D-C1.

Thus while implementations in CLT and M3D-C1 are very different, the linear and nonlinear behaviors and the maximum kinetic energy of the resistive-kink mode from the two codes are almost the same. This gives confidence in the simulation results of the resistive-kink mode. It also indicates that 2-variable reduced MHD is an adequate model for this class of problems and these parameters.

IV. Summary and discussion

In the present paper, we presented a systematic benchmarking between the CLT code and the M3D-C1 code for the linear and nonlinear tearing mode and resistive-kink mode. We find that very similar simulation results for the resistive-kink mode and the m/n=2/1 tearing mode are obtained from the two codes. We compared the linear and nonlinear growth rates, the mode structures, the nonlinear saturation levels, the Poincare plots, and the scaling laws.

CLT is an explicit finite difference code, while M3D-C1 is an implicit finite element code. Although they are both used to investigate MHD instabilities in tokamaks, they are totally different in the code implementations. As presented in the

present paper, the simulation results from the two codes are quantitatively similar. It confirms that the simulation results of the MHD instabilities are only determined by the initial conditions of the system, and are independent of the code implementations and initial perturbations. This gives us confidence in the nonlinear results of the two codes for this class of problems.

It should be noted that the simulation results from the two codes are not exactly the same. There are two possible reasons for the slight difference between the simulation results. The first reason is the different initial perturbations. In CLT, the initial perturbation only contains the n=1 component, while, in M3D-C1, random perturbations (including all the components) are applied. This is why the development of the harmonics is significantly different at the beginning of the simulations. However, there is very little qualitative influence of the initial conditions on the nonlinear evolution of the resistive-kink mode and the m/n=2/1 tearing mode. The second reason is that, due to the different implementations of the two codes, the initial profiles are slightly different. M3D-C1 first reads the initial profiles from the QSOLVER code, solves the Grad-Shafranov equation, and then generates an equilibrium consistent with its finite element representation before the simulation. However, the CLT code does not resolve the Grad-Shafranov equation. CLT reads the equilibrium data from the QSOLVER code,[23] and interpolates the data into its mesh. This means that the initial equilibria used in the two codes are slightly different, which could be a reason why the nonlinear evolution is not exactly the same.

Acknowledgment

This work is supported by the National Natural Science Foundation of China under Grant No. 11775188 and 11835010, the Special Project on High-performance Computing under the National Key R&D Program of China No. 2016YFB0200603, Fundamental Research Fund for Chinese Central Universities.

Reference

[1] T.C. Hender, J.C. Wesley, J. Bialek, A. Bondeson, A.H. Boozer, R.J. Buttery, A. Garofalo, T.P. Goodman, R.S. Granetz, Y. Gribov, O. Gruber, M. Gryaznevich, G. Giruzzi, S. Günter, N. Hayashi, P. Helander, C.C. Hegna, D.F. Howell, D.A. Humphreys, G.T.A. Huysmans, A.W. Hyatt, A. Isayama, S.C. Jardin, Y. Kawano, A. Kellman, C. Kessel, H.R. Koslowski, R.J.L. Haye, E. Lazzaro, Y.Q. Liu, V. Lukash, J. Manickam, S. Medvedev, V. Mertens, S.V. Mirnov, Y. Nakamura, G. Navratil, M. Okabayashi, T. Ozeki, R. Paccagnella, G. Pautasso, F. Porcelli, V.D. Pustovitov, V. Riccardo, M. Sato, O. Sauter, M.J. Schaffer, M. Shimada, P. Sonato, E.J. Strait, M. Sugihara, M. Takechi, A.D. Turnbull, E. Westerhof, D.G. Whyte, R. Yoshino, H. Zohm, D. the Itpa Mhd, G. Magnetic Control Topical, Chapter 3: MHD stability, operational limits and disruptions, Nuclear Fusion, 47 (2007) S128.

[2] Z. Chang, J.D. Callen, E.D. Fredrickson, R.V. Budny, C.C. Hegna, K.M. McGuire, M.C. Zarnstorff, T. group, Observation of Nonlinear Neoclassical Pressure-Gradient--Driven Tearing Modes in TFTR, Physical Review Letters, 74 (1995) 4663-4666.

[3] O. Sauter, E. Westerhof, M.L. Mayoral, B. Alper, P.A. Belo, R.J. Buttery, A. Gondhalekar, T. Hellsten, T.C. Hender, D.F. Howell, T. Johnson, P. Lamalle, M.J. Mantsinen, F. Milani, M.F.F. Nave, F. Nguyen, A.L. Pecquet, S.D. Pinches, S. Podda, J. Rapp, Control of Neoclassical Tearing Modes by Sawtooth Control, Physical Review Letters, 88 (2002) 105001.

[4] R.J. Buttery, T.C. Hender, D.F. Howell, R.J.L. Haye, O. Sauter, D. Testa, Onset of neoclassical tearing modes on JET, Nuclear Fusion, 43 (2003) 69.

[5] B. Kadomtsev, Disruptive instability in Tokamaks(helical plasma motions), Soviet Journal of Plasma Physics, 1 (1975) 389-391.

[6] B. Coppi, R. Galvao, R. Pellat, M. Rosenbluth, P. Rutherford, Resistive internal kink modes, Fizika Plazmy, 2 (1976) 961-966.

[7] Y.X. Wan, J.G. Li, Y. Liu, X.L. Wang, C. Vincent, C.G. Chen, X.R. Duan, P. Fu, X. Gao, K.M. Feng, S.l. Liu, Y.T. Song, P.D. Weng, B.N. Wan, F.R. Wan, H.Y. Wang, S.T. Wu, M.Y. Ye, Q.W. Yang, G.Y. Zheng, G. Zhuang, Q. Li, C. team, Overview of the present progress and activities on the CFETR, Nuclear Fusion, 57 (2017) 102009.

[8] R. Aymar, P. Barabaschi, Y. Shimomura, The ITER design, Plasma Physics and Controlled Fusion, 44 (2002) 519.

[9] H.P. Furth, J. Killeen, M.N. Rosenbluth, Finite-resistivity instabilities of a sheet pinch, The physics of Fluids, 6 (1963) 459-484.

[10] P.H. Rutherford, Nonlinear growth of the tearing mode, The Physics of Fluids, 16 (1973) 1903-1908.

[11] R.B. White, D.A. Monticello, M.N. Rosenbluth, B.V. Waddell, Saturation of the tearing mode, The Physics of Fluids, 20 (1977) 800-805.

[12] F. Porcelli, D. Boucher, M.N. Rosenbluth, Model for the sawtooth period and amplitude, Plasma Physics and Controlled Fusion, 38 (1996) 2163.

[13] R.E. Denton, J.F. Drake, R.G. Kleva, D.A. Boyd, Skin Currents and Compound Sawteeth in Tokamaks, Physical Review Letters, 56 (1986) 2477-2480.

[14] A.Y. Aydemir, J.C. Wiley, D.W. Ross, Toroidal studies of sawtooth oscillations in tokamaks, Physics of Fluids B: Plasma Physics, 1 (1989) 774-787.

[15] H. Lütjens, J.-F. Luciani, XTOR-2F: a fully implicit Newton–Krylov solver applied to nonlinear 3D extended MHD in tokamaks, Journal of Computational Physics, 229 (2010)

8130-8143.

[16] C.R. Sovinec, J.R. King, Analysis of a mixed semi-implicit/implicit algorithm for low-frequency two-fluid plasma modeling, Journal of Computational Physics, 229 (2010) 5803-5819.

[17] S.C. Jardin, N. Ferraro, X. Luo, J. Chen, J. Breslau, K.E. Jansen, M.S. Shephard, The M3D-C1approach to simulating 3D 2-fluid magnetohydrodynamics in magnetic fusion experiments, Journal of Physics: Conference Series, 125 (2008) 012044.

[18] O. Czarny, G. Huysmans, Bézier surfaces and finite elements for MHD simulations, Journal of Computational Physics, 227 (2008) 7423-7445.

[19] H.W. Zhang, J. Zhu, Z.W. Ma, G.Y. Kan, X. Wang, W. Zhang, Acceleration of three-dimensional Tokamak magnetohydrodynamical code with graphics processing unit and OpenACC heterogeneous parallel programming, International Journal of Computational Fluid Dynamics, 33 (2019) 393-406.

[20] I. Krebs, S.C. Jardin, S. Günter, K. Lackner, M. Hoelzl, E. Strumberger, N. Ferraro, Magnetic flux pumping in 3D nonlinear magnetohydrodynamic simulations, Physics of Plasmas, 24 (2017) 102511.

[21] S. Wang, Z. Ma, Influence of toroidal rotation on resistive tearing modes in tokamaks, Physics of Plasmas, 22 (2015) 122504.

[22] L. Duan, X. Wang, X. Zhong, A high-order cut-cell method for numerical simulation of hypersonic boundary-layer instability with surface roughness, Journal of Computational Physics, 229 (2010) 7207-7237.

[23] J. DeLucia, S.C. Jardin, A.M.M. Todd, An iterative metric method for solving the

inverse tokamak equilibrium problem, Journal of Computational Physics, 37 (1980) 183-204.

[24] H.P. Furth, P.H. Rutherford, H. Selberg, Tearing mode in the cylindrical tokamak, The Physics of Fluids, 16 (1973) 1054-1063.